Earth and Planetary Science Letters 307 (2011) 395–408

Contents lists available at ScienceDirect

Earth and Planetary Science Letters

journal homepage: www.elsevier.com/locate/epsl

Mineralogical heterogeneities in the Earth's mantle: Constraints from Mn, Co, Ni and Zn partitioning during partial melting

V. Le Roux [a,b,*], R. Dasgupta [a], C.-T.A. Lee [a]

[a] Department of Earth Science, Rice University, MS-126, 6100 Main Street, Houston, TX 77005, USA
[b] Woods Hole Oceanographic Institution, 266 Woods Hole Road, Woods Hole, MA 02543-1050, USA

ARTICLE INFO

Article history:
Received 16 November 2010
Received in revised form 28 April 2011
Accepted 8 May 2011
Available online 1 June 2011

Editor: L. Stixrude

Keywords:
transition metals
mineralogical heterogeneities
peridotite mantle
eclogite
basalts

ABSTRACT

The first-row transition elements (FRTEs) are compatible to moderately incompatible during melting in mafic and ultramafic systems. Unlike highly incompatible elements, FRTEs are sensitive to changes in mineralogy or major element composition, and thus, are promising to trace lithological heterogeneities in the mantle source regions of basaltic magmas. However, experimental constraints on the partitioning behaviors of several FRTEs at mantle conditions, such as Zn, are still lacking despite growing interest in the application of these tracers to magmatic systems. Here we present mineral-melt partitioning experiments at 1.5–2.0 GPa and 1300–1500 °C for divalent FRTEs—Zn, Fe, Mn, Co, and Ni. Our study provides for the first time Zn and Zn/Fe fractionation data between peridotitic olivine, orthopyroxene, clinopyroxene and basaltic melt. Using our new partition coefficients and combining multiple ratios (Zn/Fe, Ni/Co, Mn/Fe, and Mn/Zn) we assess the role of FRTEs as tracers of mineralogical composition in the mantle source regions of basalts. We show that, during melting, olivine and orthopyroxene do not significantly fractionate Mn, Fe, and Zn from each other, and because olivine and orthopyroxene dominate the budget of these elements in ultramafic systems, melts from peridotite would be expected to have similar Mn/Fe and Zn/Fe as the source. In contrast, our results for clinopyroxene and published results for garnet show strong fractionations, such that melts of pyroxenites or eclogites would be expected to have low Mn/Fe, Co/Fe, Ni/Co, Mn/Zn and high Zn/Fe compared to peridotite partial melts. We compare Zn, Fe, Co, Mn and Ni contents of natural oceanic basalts to modeled compositions of peridotitic and pyroxenitic partial melts. Most mid-ocean ridge basalts (MORB) and near-ridge ocean island basalts (OIB, e.g., Iceland and Galapagos) can be explained by shallow melting of peridotite, but most ocean island basalts away from ridges deviate from predicted peridotite melt compositions. We use melting and mixing models of FRTEs ratios in peridotite and in MORB-like eclogite to illustrate the potential contribution of eclogite- and peridotite derived melts in individual MORB and OIB lavas. We also present a simple melt–melt mixing model that estimates the amount of eclogite in the source of mantle end-members HIMU, EM1, and EM2 and individual OIB.

1. Introduction

A large number of studies have used trace element and radiogenic isotopic systems in mafic and ultramafic rocks to show that the source regions of mantle-derived basalts are highly heterogeneous (e.g., Hofmann, 1997; Weaver, 1991; Willbold and Stracke, 2006; Zindler and Hart, 1986). However, because most of the trace elements investigated in such studies are highly incompatible elements and because radiogenic isotopic systems are ultimately based on the same set of incompatible elements, they do not track heterogeneities in terms of mineralogy.

There have been a number of hypotheses to explain the major and trace element composition of the source regions of mantle-derived basalts. In particular, it has been shown that the composition of mid-ocean ridge basalts (MORB) cannot be accurately reproduced by melting of peridotite alone (e.g. Kushiro, 2001), and that pyroxene-rich veins in the source of MORB could account for their garnet signature (e.g. Hirschmann and Stolper, 1996). Similarly, the source of ocean island basalts (OIB) may contain mineralogical heterogeneities, i.e., lithologies distinct from a primitive mantle (PM)-like peridotite because melts derived from partial melting of a PM-like peridotite cannot reproduce the low Al_2O_3 and high FeO contents of many alkalic OIB (Dasgupta, et al., 2010; Hirschmann, et al., 2003; Kogiso and Hirschmann, 2006), and the low SiO_2 and high CaO of "HIMU", high time-integrated U/Pb reservoirs, (e.g. Kogiso, et al., 1998) or high SiO_2 and K_2O of "enriched mantle" ("EM") end-members (e.g. Jackson and Dasgupta, 2008; Spandler, et al., 2010).

Based on experimental constraints, it has been suggested that pyroxenites and/or amphibolites melts contribute to the diversity of OIB compositions, which range from highly alkalic, silica-poor basalts

* Corresponding author at: Woods Hole Oceanographic Institution, 266 Woods Hole Road, Woods Hole, MA 02543-1050, USA.
E-mail address: vleroux@whoi.edu (V. Le Roux).

0012-821X/$ – see front matter © 2011 Elsevier B.V. All rights reserved.
doi:10.1016/j.epsl.2011.05.014

to silica-rich tholeiites. Thus, the source of OIB may contain silica-poor garnet pyroxenite or bi-mineralic eclogite (e.g., Kogiso, et al., 2003; Kogiso and Hirschmann, 2006), carbonated eclogites/pyroxenites (Dasgupta, et al., 2006; Gerbode and Dasgupta, 2010), silica-rich high-Mg pyroxenites (Herzberg, 2006) or amphibolites (Pilet, et al., 2008). Based primarily on the Fe–Si relationship of basalts versus experimental melts, Dasgupta et al. (2010) proposed that silica-excess MORB-pyroxenites and carbonated MORB-pyroxenites may globally represent the two additional lithologies in the Earth's peridotite mantle.

However, despite these advances in interpreting major element chemistries of basalts, arguments based solely on major elements struggle to distinguish between eclogite/pyroxenitic sources and metasomatized peridotite sources (e.g., Dasgupta, et al., 2007; Niu and O'Hara, 2003; Pilet, et al., 2005) as similar major element signatures may be derived from both sources. In addition, major elements can be strongly affected by crystal fractionation or re-equilibration at temperatures and pressures different from that of original melting in the mantle. Thus, an independent approach is desirable for identifying mineralogical heterogeneities in the mantle source. Here, we explore the use of first-row transition elements (FRTEs) as tracers of source mineralogy. Because of their moderately incompatible to compatible behavior, FRTEs appear suitable to trace source mineralogy. In particular, ratios like Mn/Fe and Zn/Fe are minimally affected by partial melting in peridotite or by cryptic metasomatism (Humayun et al. 2004, Le Roux et al. 2010), but more experiments are needed to confirm this hypothesis. The objective of this paper is to experimentally constrain the partition coefficients of some key FRTEs and explore a combination of FRTEs ratios (Zn/Fe, Mn/Fe, Co/Fe, and Ni/Co) to track and quantify clinopyroxene (Cpx) ± garnet (Gt) rich assemblages versus olivine (Ol) ± orthopyroxene (Opx) rich assemblages in the source of basalts.

A few studies have used FRTEs as tracers of mineralogical heterogeneities in the mantle. Humayun et al. (2004) and Qin and Humayun (2008) used Fe/Mn ratios to argue for Fe enrichment in the source of Hawaiian lavas. They attributed the Fe enrichment to outer core contribution. Prytulak and Elliott (2007) suggested that most OIB have Ti contents too high to be derived from partial melting of peridotite only, and thus, invoke the contribution of recycled crust in their source. Sobolev et al. (2007; 2005) showed that the transition metal contents (e.g. Ni and Mn) of olivine phenocrysts in OIB lavas cannot be reconciled with peridotite-derived melt and suggested that the Earth's mantle contains variable quantities of hybrid pyroxenites formed through reaction between peridotite and eclogites melts. Based on the same observations, Wang and Gaetani (2008) proposed that a simple mixing of basaltic and reacted eclogitic melt can reconcile the features observed in Sobolev et al. (2007).

Despite the growing interest in FRTEs behavior, there is still no complete set of partitioning data for all these elements. Although data for elements such as Ti, Mn, Fe and Ni are abundant (e.g. Beattie, et al., 1991; Dunn, 1987; Hart and Davis, 1978; Li and Ripley, 2010; Prytulak and Elliott, 2007), partitioning of other FRTEs such as Zn are not experimentally constrained. Recently, it has been suggested that Zn/Fe ratios could help distinguishing olivine-rich lithologies from Cpx-garnet rich lithologies (Le Roux, et al., 2010; Lee, et al., 2010). However, they relied mostly on indirect estimates of partition coefficients during mantle melting.

Here we present experimental partition coefficients of FRTEs Mn, Fe, Co and Ni in Ol-melt, Opx-melt, and Cpx-melt pairs at shallow upper mantle conditions (<2 GPa), and the first experimental data on Zn partitioning in peridotitic minerals-basaltic melt systems. In the range of typical fO_2 of the Earth's upper mantle, the transition metals Mn, Co, Ni and Zn are primarily found in their +2 valence states, hence are likely to substitute for Fe^{2+} and/or Mg^{2+}. Combining our internally consistent partitioning data for Ol-melt, Opx-melt, and Cpx-melt with previous studies, we estimate bulk partition coefficients during mantle melting and assess how the combination of multiple FRTEs (Zn–Mn–Fe–Co–Ni) systematics can trace mineralogical heterogeneities in the mantle. In particular we use Zn/Fe versus Mn/Fe, Co/Fe versus Mn/Fe, and Ni/Co versus Mn/Zn to constrain the distribution of Cpx-Gt rich heterogeneities in the source of mantle-derived basalts.

2. Methods

2.1. Starting material

In order to achieve mineral-melt equilibria with appropriate range of phase assemblage and phase compositions relevant for shallow mantle melting, we have used three different starting materials doped with different amounts of transition metals (including Mn, Co, Ni and Zn) with concentration in the form of total oxides ranging from ~1 to ~2.5 wt.%. The first starting material (Mix1) is a mixture between natural mid-Atlantic ridge (MAR) basalt powder (~70%) and KLB-1 peridotite powder (~30%) doped with ~1 wt.% "transition metals" oxides (Sc, V, Cr, Mn, Co, Ni, Cu, Zn, and Ge). Both the MAR and KLB-1 powders were dehydrated in a reducing (QFM-1.5, where QFM is the quartz–fayalite–magnetite buffer) $CO–CO_2$ atmosphere at 1000 °C for >10 h. The two powders were then mixed thoroughly using an agate mortar, under ethanol, and stored in a 100 °C oven until use. The relative concentration of transition metals in the mix was chosen according to published partition coefficients where available. The second starting material (Mix2) is 100% of the MAR basalt powder. It was doped with ~2.5 wt.% oxides of the transition metal mix used for Mix1, except that Ga was added into the mix. The third starting material (Mix3) is a synthetic basalt reconstructed using reagent grade oxides powders. All major elements except Fe were mixed together in an agate mortar and dried at 1000 °C overnight. Fe as Fe_2O_3 was subsequently added. To convert all Fe^{3+} in this starting material to Fe^{2+}, the final mix was placed in a gas mixing furnace at 1000 °C and fO_2 of QFM-1.5 overnight. The major element powder was then doped with ~1.3 wt.% oxides of the same transition metal mix used for Mix2. The major and trace element compositions of Mix1, 2, and 3 were verified by making glasses of all the three compositions using a piston cylinder and then by analyzing the glasses using EPMA and LA–ICP-MS.

2.2. Experimental procedure

Partitioning experiments were carried out using an end-loaded piston cylinder device at the Experimental Petrology Laboratory of Rice University (USA), following the calibration of Tsuno and Dasgupta (2011). A total of 10 experiments at temperature and pressure conditions ranging from 1290 °C to 1500 °C and 1.5 GPa to 2 GPa were performed. We used a half-inch $BaCO_3$ assembly with graphite capsules, MgO spacers, straight-walled graphite heaters, and thermocouple wires housed in four-bore, dense alumina sleeves. Pb-foils were used to contain the friable $BaCO_3$ assembly and to provide lubrication between the assembly and the bore of the pressure vessel. The assembly parts were dried overnight (MgO spacers at 1000 °C; graphite capsule at 300 °C; graphite furnace at 100 °C) before use to achieve nominally anhydrous conditions. The use of graphite capsules ensured the maintenance of oxygen fugacity close to the CCO buffer ($C + O_2 = CO_2$), which is known to yield oxygen fugacity similar to Earth's shallow upper mantle (e.g., Medard, et al., 2008), and under these conditions, the valence state of the targeted FRTEs should be dominantly +2. The temperature was monitored and controlled with a $W_{95}Re_5$-$W_{74}Re_{26}$ thermocouple, within ±1 °C. The pressure was maintained by a pressure holding device within 0.01 GPa. Considering the uncertainty in the pressure calibration and the thermal gradient in our half-inch assembly (Tsuno and Dasgupta, 2011), the experimental P–T uncertainties are thought to be ±0.1 GPa and ±10 °C. Our experimental duration varied from 22 to 67 h. The experiments were terminated by turning off power to the heater and then by slowly depressurizing the assembly. The recovered run products were

mounted in epoxy resin and polished using alumina lapping film and alumina paste on soft nylon cloth. Water was used as lubricant. Experimental conditions are summarized in Table 1.

2.3. Analytical techniques

Experimental products were analyzed using a CAMECA SX-50 electron probe microanalyzer (EPMA) at Texas A&M University (USA). Motivated by the work of Sobolev et al. (2005, 2007), we measured both major elements and trace elements using electron microprobe. The choice of electron microprobe as the analytical tool, which has spatial resolution of <5 micron, for trace element analysis meant that we could perform conventional, phase equilibria experiments, without the need of growing big crystals. Indeed many of our mineral silicates were too small for ablative techniques (e.g., LA–ICPMS and SIMS) that are commonly used for trace element analyses. Major element analyses in silicate minerals and melts were performed using an accelerating voltage of 15 kV, a beam current of 10 nA and 60 s peak counting time. Trace elements were analyzed using an accelerating voltage of 20 kV, a beam current of 300 nA and 60 s peak counting time. The beam diameter was 1–3 μm for silicates and ~20 μm for quenched melts. The reproducibility of major elements is ~1% (1 σ_{SD}) and 5 to 10% for trace elements.

The data quality of trace element concentrations measured using EPMA was verified through in-situ LA–ICPMS analyses on seven experimental charges previously analyzed by EPMA. We used a Thermo-Finnigan Element Sector ICP-MS coupled with a New Wave 213 nm laser ablation system at Rice University (USA). Analyses were carried out in medium mass resolution ($m/\delta m = 3000$), using a 100 μm LASER spot size for experimental charges and 55 μm for external standards. The energy density ranged between 15 and 20 J/cm^2 and the repetition rate was set at 10 Hz. Sensitivity was typically estimated at about 350,000 cps/ppm for La on a BHVO2 glass standard using a 55 μm laser beam at 10 Hz (15.6 ppm of La; Gao, et al., 2002). Drift associated with ablation yield or matrix effects was controlled by internal normalization (Longerich et al., 1996) using ^{30}Si. For this study we focused on the measurements of ^{55}Mn, ^{57}Fe, ^{59}Co, ^{60}Ni and ^{66}Zn. The external reproducibility and accuracy of the measurements were checked using BHVO2G, BCR2G and NIST610 standards. The detection limit was estimated at three times the standard deviation of the background divided by the sensitivity. For additional details on the LA–ICPMS technique the reader is referred to Lee et al. (2008).

Table 1
Experimental conditions, phase assemblages and available phase abundances in the experiments.

Run no.	P (Gpa)	T (°C)	Duration (h)	Melt fraction	Ol	Opx	Cpx	Sum r^2
Starting composition Mix1								
G90	1.5	1375	67	0.49	—	0.51	—	1.28
G92	1.5	1425	24	+	—	+	—	
G83	2	1400	40	0.52	—	0.48	—	1.24
G81	2	1450	22	0.61	0.04	0.35	—	0.96
G84	2	1500	24	0.65	0.02	0.33	—	0.64
Starting composition Mix2								
G94	1.5	1290	24	0.40	—	—	0.60	1.88
G93	1.5	1320	23	0.55	—	—	0.45	0.88
Starting composition Mix3								
G109	1.5	1300	24	0.42	0.16	0.01	0.41	2.6
G110	1.5	1310	22	0.46	0.1	0.01	0.41	0.13
G107	1.5	1325	23	0.44	0.03	0.25	0.28	1.89

Major element starting compositions are detailed in Table 2 of Supplementary material, trace elements in Table 2. Sum r^2 is the sum of the squared oxide residuals obtained using the modes, phase compositions, and the bulk starting compositions. Sum r^2 are indicated for the experiments where compositions of all the phases observed were available. '+' indicates that the phase is present, '—'indicates that the phase is absent. G110 is the only crystallization experiment: P = 1.5 GPa, initial temperature, T_i = 1600 °C, final temperature, T_f = 1310 °C, ramp down rate from T_i to T_f of 1 °C/min and duration at T_f of 22 h.

3. Results

3.1. Phase assemblages, textures, and major element compositions of experimental phases

Experimental conditions and phase assemblages are summarized in Table 1 and major element oxide compositions of melts and minerals are listed in Table 2 of Supplementary material. Our experiments yield the following assemblages: Opx ± Ol + melt for "Mix1" starting composition, Cpx + melt for "Mix2" starting composition and Opx + Cpx + Ol + melt for "Mix3" starting composition. All the experiments produced large quenched melt pool coexisting with silicate minerals. The static phase equilibria experiments (fixed T) produced olivine crystals ≤ 50–70 μm diameter and Cpx and Opx ≤ 30 μm. The single crystallization experiment (G110), on the other hand, produced Cpx crystals measuring up to 500 μm and Opx up to 200 μm diameter. BSE images showed a 5–10 μm wide rims on the edge of the crystals in this experiment, which we interpret as re-equilibration during quench. Measurements have been systematically performed in the mineral cores. The chemical variability in large Cpx appears fairly limited with standard deviations that are similar to the ones observed in smaller grains from other experiments. Also, trace element partitioning data between Cpx and melt from experiment G110 is in good agreement with other experiments including smaller Cpx grains. No visible zoning have been observed in other experiments.

Our experimental Ol, Opx and Cpx major element compositions fall within the range of previously reported compositions for peridotitic minerals in experiments performed at similar pressure–temperature conditions (e.g. Falloon, et al., 2008; Kinzler, 1997; Kinzler and Grove, 1992; Kogiso, et al., 1998; Wasylenki, et al., 2003). For example, Al_2O_3 and CaO contents of Cpx from 1.6 GPa, peridotite multiple saturation experiments of Kinzler and Grove (1992) are ~7.4–10.5 wt.% and 10–12 wt.%, respectively, and those from our experiments vary from 7.4 to 10.7 wt.% and 10.7 to 15.4 wt.%, respectively. The MgO contents of clinopyroxene in experiment G93 and G94 (15 and 13.5 wt.% respectively) are, however, somewhat lower compared to previously reported peridotitic compositions that range between 17 and 23 wt.% MgO. From the standpoint of MgO contents, our Cpx compositions are between peridotitic and eclogitic clinopyroxenes (e.g. eclogitic Cpx in Pertermann, et al., 2004 vary from 7 to 11 wt.% MgO). Further, Al_2O_3 content (4–9 wt.%) and Mg# (82–92) of our experimental Opx span the range observed in the previous experiments under similar conditions and for peridotitic bulk compositions. For instance, Walter (1998) reports Al_2O_3 content in Opx of 3–8 wt.% and Mg# of 90–93 at 3 GPa.

3.2. Chemical equilibrium and data quality

We assessed the approach to chemical equilibrium between the different phases by calculating the exchange partition coefficient $K_{DFe/Mg}$ between minerals and melts (e.g. for olivine $K_{D_{Fe/Mg}} = \frac{X^{melt}_{Fe2+} / X^{Ol}_{Fe2+}}{X^{melt}_{Mg} / X^{Ol}_{Mg}}$). They are reported in Table 3. $K_{D_{Fe/Mg}}$ between olivine and basaltic melts in our experiments range from 0.33 to 0.35, which is in good agreement with previously published values (Kushiro, 2001; Kushiro and Walter, 1998; Roeder and Emslie, 1970; Walter, 1998). The measured $K_{DFe/Mg}$ between orthopyroxene and basaltic melt are between 0.29 and 0.36, also consistent with previous studies (e.g. Kinzler and Grove, 1992; Parman and Grove, 2004; Walter, 1998). Additionally the residual squares of the mass balance calculations available for most experiments (calculated by using the major element compositions of all phases and

the modal proportions that give minimum residual squares) are reasonably good, indicating a close system in the experiments.

The quality of EPMA trace element data has been checked through combined LA–ICPMS analyses in seven experiments. We measured trace elements by LA–ICPMS in six glasses with varying amount of transition metals and in large clinopyroxenes obtained through a crystallization experiment (Fig. 1a). As shown in Fig. 2, there is a good 1:1 correlation between the two techniques, regardless of the initial concentration of Mn, Co, Ni and Zn. The only slight discrepancy was in experiment G81 where Zn concentrations between EPMA and LA–ICPMS in the quenched melt were not in agreement. We think that EPMA analyses were unable to sample heterogeneities in quenched dendrites in this experiment. Hence, we used the Zn concentration obtained using LA–ICPMS to calculate $D_{Zn}^{mineral/melt}$ for this particular experiment. Some of our experiments display both glassy and dendritic parts in the quenched melt pool. For calculating the *Ds*, we particularly used the homogeneous glassy part (except G81 that has no glassy domain). However no significant difference in *Ds* was observed using the dendritic melt phases.

To ensure quality measurements with the electron microprobe, we doped our experiments with a mix of transition metals powder including Mn, Co, Ni and Zn. Trace elements analyses are reported in Table 2. The total weight percent oxide of this transition metal mix varies in minerals from 0.56% to 3.22% and in the glass phase from 0.98% to 2.32%. Those totals also include all other 'transition metals' added in the mix (Cr, Cu, V, Sc, Ge, and Ga) but we focus here on elements that are dominantly in their +2 valence state in the Earth's mantle and can potentially substitute with Fe^{2+} or Mg^{2+}. Although some of our compositions were doped significantly with transition metals, there is no systematic variation of $D_{Co}^{mineral/melt}$ $D_{Ni}^{mineral/melt}$ and $D_{Zn}^{mineral/melt}$ with the Co, Ni and Zn content of the phases respectively (Fig. 1 Supplementary material). This suggests that those elements behave as trace elements in the mineral phase of interest and their distribution follow Henry's law (they are infinitely diluted in the system, thus non-ideal effects can be ignored, hence their activity and concentration are linearly correlated). $D_{Mn}^{Opx/melt}$ is observed to increase with increasing Mn in the Opx (Fig. 1a Supplementary material) but such correlation goes away when we select experiments with similar temperature conditions. This demonstrates that the positive correlation between $D_{Mn}^{Opx/melt}$ and Mn concentration in Opx is caused by the strong temperature dependence of $D_{Mn}^{Opx/melt}$ rather than deviation from Henry's law.

3.3. Mineral-melt partition coefficients of first-row divalent cations

The D values of Zn, Mn, Co, and Ni between Ol, Opx, Cpx and melt are reported in Table 3 and plotted as a function of temperature in Fig. 3. We are not able to assess at this point whether partition coefficients between clinopyroxene and melt have any temperature dependence as the temperature range for Cpx-melt equilibria was too narrow for our experiments. However we observe strong temperature dependence for olivine-melt and Opx-melt partition coefficients. $D_{Mn}^{Ol/melt}$ and $D_{Mn}^{Opx/melt}$ both decrease with increasing temperature (Fig. 3). The well-known temperature dependence of $D_{Fe}^{Ol/melt}$ and $D_{Fe}^{Opx/melt}$ (e.g. Roeder and Emslie, 1970) is also observed in our dataset. Our experiments record slight temperature dependence for $D_{Co}^{Opx/melt}$ and $D_{Ni}^{Opx/melt}$ whereas both $D_{Co}^{Ol/melt}$ and $D_{Ni}^{Ol/melt}$ decrease strongly with increasing temperature. D_{Zn} shows a slight temperature dependence and it is possible that the larger scatter in Zn data may obscure some of the temperature-dependency.

3.4. Mineral-melt exchange K_Ds of first-row transition metals

Our experiments demonstrate notable temperature dependence of olivine-melt and Opx-melt partition coefficients for Mn, Fe, Co, Ni, and Zn. However, we observe that owing to similar temperature dependence of mineral-melt *Ds* for many of these transition metals, the ratio of *Ds* may be less sensitive to temperature and hence likely vary little during differentiation. We test this by defining mineral-melt exchange coefficients, K_Ds for first-row, divalent cation pairs of choice, Mn–Fe, Zn–Fe, Co/Fe, Mn–Zn, and Ni–Co and plotting them as a function of reciprocal temperature (Fig. 4).

In Fig. 4 we show that, for Mn–Fe and Mn–Zn, Cpx-melt K_Ds are distinctly higher than olivine-melt and Opx-melt K_Ds. Similarly, Cpx-melt K_D for Zn–Fe is lower than those of olivine-melt and Opx-melt. $K_{DZn/Fe}^{mineral/melt}$ and $K_{DMn/Fe}^{mineral/melt}$also do not show any clear temperature dependence, which is consistent with previous suggestions (Humayun, et al., 2004; Le Roux, et al., 2010; Walter, 1998). We note, however, that in two of our relatively lower temperature experiments (G107 and G109) the olivine-melt Zn/Fe K_D to be noticeably lower and only slightly higher than Cpx-melt Zn–Fe K_D (Fig. 4). It is not clear at present whether lower Zn–Fe Ol-melt and Opx-melt K_D in these two experiments are an effect of temperature or bulk composition. Similar to our observation on Zn–Fe mineral-melt K_Ds, we show that Mn–Zn, Co–Fe and Ni–Co mineral (olivine, Opx, and

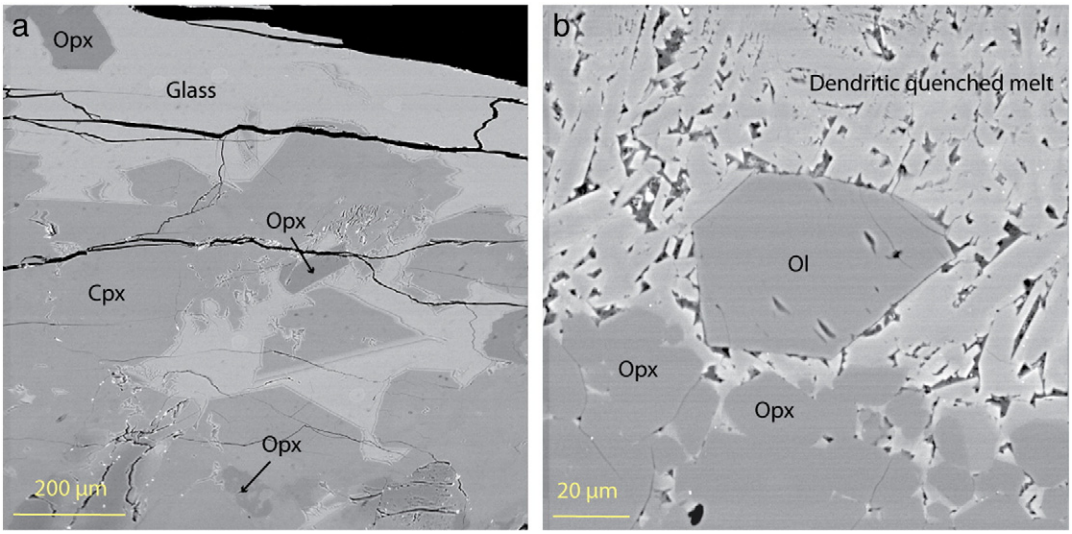

Fig. 1. Back-scattered electrons (BSE) image of (a) a crystallization experiment (G110: P = 1.5 GPa, initial temperature, T_i = 1600 °C, final temperature, T_f = 1310 °C, ramp down rate from T_i to T_f of 1 °C/min and duration at T_f of 22 h) where >100 microns dimension Cpx and Opx coexist with a glassy quenched melt phase and (b) a multiple-saturation experiment (G81: P = 2 GPa, 1450 °C, 22 h) showing contact between a dendritic quenched melt phase and crystals of Opx and a euhedral crystal of olivine.

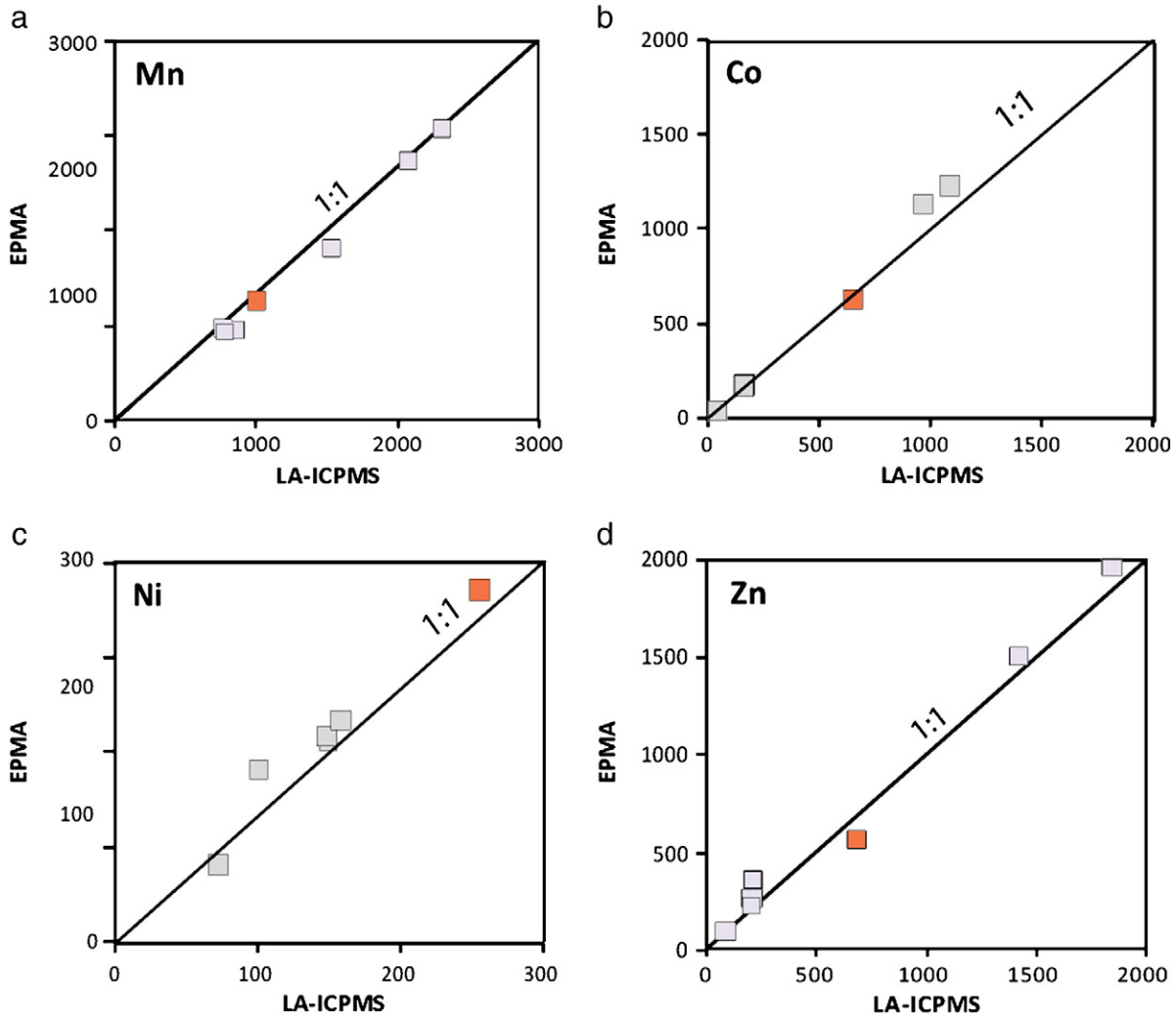

Fig. 2. Concentrations of Mn (a), Co (b), Ni (c), and Zn (d) measured by electron probe micro analyzer (EPMA) versus the same measured using laser ablation inductively-coupled mass spectrometer (LA–ICPMS) in the same experimental charges. The plots demonstrate very good agreement between the two analytical techniques. The gray squares are average measurements made in quenched glasses (experiment numbers: G81, G84, G92, G94, G99, and G100) and the orange square represents average measurements made in clinopyroxenes from experiment G110. The solid black line is the 1:1 ratio line.

Cpx)-melt K_Ds have limited temperature dependence, hence making them potentially useful for testing equilibrium and for constraining melt composition in equilibrium with a known source.

4. Discussion

4.1. Comparison of our mineral-melt Ds and mineral-melt exchange K_Ds with literature data

Partition coefficients between mineral and melt from this study are compared with published data in Figs. 5 and 6. In Fig. 5, mineral-melt partition coefficients $D_{element}^{mineral/melt}$ for a given element are plotted against mineral-melt partition coefficients for Fe, $D_{Fe}^{mineral/melt}$. Exchange coefficient isopleths are shown for reference. In Fig. 6, we have plotted individual D values in the order of increasing compatibilities for all phases.

Zn^{2+}: There are few available data on Zn partitioning in mafic and ultramafic mantle rocks. Pertermann et al. (2004) reported Zn partition coefficients between clinopyroxene, garnet and melt in anhydrous MORB-like eclogite and showed that, in the P–T range of 2.9–3.1 GPa and 1325 °C–1390 °C, $D_{Zn}^{Cpx/melt}$ varies between 0.64 and 0.7. Our $D_{Zn}^{Cpx/melt} = 0.48 \pm 0.03$ measured at 1.5 GPa and ~1300 °C indicate that either Zn is more incompatible in peridotitic clinopyroxene or $D_{Zn}^{Cpx/melt}$ increases with increasing pressure. We note, however, that $K_{DZn/Fe}^{Cpx/melt}$ yields similar values in eclogite and peridotite bulk compositions, i.e. ~0.7 in Pertermann et al. (2004) and 0.67 ± 0.03 in peridotitic Cpx (this study). This suggests that Zn/Fe exchange between clinopyroxene and basaltic melt is similar over the range of pressure, temperature and compositions relevant for the Earth's shallow upper mantle. Kohn and Schofield (1994) reported $D_{Zn}^{Ol/melt}$ ranging from ~0.77–1 at similar temperature conditions to our experiments but at 1-bar and for a Fe-free system, which is consistent with our determined value of 1.04 ± 0.12. This might further suggest that Zn partitioning between olivine and melt does not vary strongly with pressure and bulk compositions.

Fe^{2+}: Our Fe partitioning data compare very well with the data of Walter (1998) at 3 GPa and 1530 °C (experiment 30.07; $D_{Fe}^{Ol/melt} = 1$). The average $D_{Fe}^{Ol/melt}$ of our experiments is 1.28 ± 0.26 but it includes experiments that have been performed at lower temperatures hence $D_{Fe}^{Ol/melt}$ is expected to be higher. Our experiments at 1450 °C and 1500 °C yield $D_{Mn}^{Ol/melt} = 1.06 \pm 0.05$, which is in agreement with Walter (1998). Similarly, $D_{Fe}^{Opx/melt}$ are fairly consistent with the experiments of Walter (1998) ($= 0.58$ in experiment 30.07; $= 0.69 \pm 0.04$ in our study for experiments at ≥1450 °C). $D_{Fe}^{Cpx/melt}$ in our study was only

Table 2
Concentrations (in ppm unless specified) of Mn, Co, Ni and Zn in bulk starting compositions (start. comp.), experimental phases, and isotopic mantle end-member basalts.

	Mn	Stdev	Co	Stdev	Ni	Stdev	Zn	Stdev		Mn	Stdev	Co	Stdev	Ni	Stdev	Zn	Stdev
Start. comp.									*Melt*								
Mix1*	679	38	209#		451#		149	27	G81*	730	20	183	15	167	21	353	60
MIx2**	2306	30	1320	27	538	49	1502	114	*G81**	*761*	*20*	*180*	*20*	*150*	*18*	*208*	*1*
*Mix2***	*2316*	*70*	*1100*	*30*	*450*	*60*	*1422*	*22*	G84*	708	36	178	13	170	22	260	47
Mix3***	804	79	718	46	222	50	824	31	G84*	849	42	170	5	150	8	204	25
									G88*	693	21	170	19	259	41	323	40
Olivine									G90*	685	13	160	8	193	22	235	25
G81*	569	23	411	16	1107	21	227	14	G92*	698	21	170	18	175	6	223	43
G84*	534	31	348	13	960	73	232	30	*G92**	*778*	*40*	*170*	*5*	*160*	*20*	*201*	*9*
G107***	876	25	1932	13	1004	50	1112	40	G93**	2296	39	1352	31	294	15	1736	69
G109***	896	27	1774	292	874	50	1157	12	G94**	2056	44	1222	30	136	46	1964	85
									*G94***	*2073*	*150*	*1000*	*30*	*130*	*10*	*1845*	*140*
Opx									G107***	848	24	628	21	110	50	1094	54
G81*	510	39	182	29	748	181	140	27	G109***	777	14	580	14	85	20	997	53
G83*	610	18	218	15	638	81	183	48	G110***	820	7	602	19	82	10	1128	32
G84*	464	65	158	28	660	169	164	33									
G90*	583	21	208	13	693	60	180	14	*Cpx*								
G92*	545	13	170	14	653	95	133	17	G93**	2438	50	1428	36	990	158	816	52
G107***	760	65	774	50	1350	695	622	40	G94**	2378	72	1446	27	514	84	980	44
G109***	814	18	844	26	368	26	718	71	G107***	920	73	600	29	268	55	484	29
G110***	800	14	854	20	364	79	784	25	G110***	946	54	628	36	220	27	558	52
									*G110****	*1001*	*5*	*650*	*50*	*190*	*50*	*682*	*150*

Mantle

	Mn	Co	Ni	Zn	Fe (wt.%)
End-members					
HIMU	1642	77	342	112	10.10
EM1	1158	69	439	114	8.46
EM2	1300	90	353	107	8.30

Ol, Opx, Cpx and melts have been analyzed primarily by EPMA. LA–ICP-MS analyses for some samples are shown for comparison (marked as italicized text). The # symbol against reported elemental concentrations in the starting mixes indicates that the concentrations of those elements have been estimated both using EPMA analyses of a synthesized glass and by weighing. * indicates starting composition of Mix1, ** indicates starting composition of Mix2, *** indicates starting composition of Mix3. At the bottom are the calculated Mn, Co, Ni and Zn concentrations of mantle end-member basalts HIMU, EM1 and EM2 from the compilation of Jackson and Dasgupta (2008). Values for Co and Ni have been recalculated for basalt MgO = 14 wt.%.

measured at ~1300 °C and are slightly higher (= 0.71 ± 0.04) than in the experiment of Walter (1998) (= 0.54) at 1530 °C and 3 GPa.

Mn^{2+}: Among other studies, Watson (1977), Dunn (1987), and Walter (1998) measured Mn partition coefficient between olivine and basaltic liquid. Watson (1977) showed that Mn partitioning in forsterite is strongly temperature and melt composition dependent (especially at low temperatures ~1250 °C), with $D_{Mn}^{Ol/melt}$ increasing with SiO_2 content of the melt. They report $D_{Mn}^{Ol/melt}$ of 0.50–0.67 for SiO_2 content in the melt ranging from 43 wt.% to 59 wt.%, respectively, at 1450 °C. In experiment G81 (T = 1450 °C; SiO_2 = 46.6 wt.%) >we find $D_{Mn}^{Ol/melt}$ = 0.78, which is slightly higher than their values. Dunn (1987) reported $D_{Mn}^{Ol/melt}$ from 1-bar experiments, varying from 1.38 ± 0.04 at 1177 °C to 1.53 ± 0.06 at 1150 °C, which is slightly higher than what we observe in our experiments (average = 0.93 ± 0.20). However the SiO_2 contents of the melts in our experiments are lower and our experiments were performed at temperatures ranging from 1300 °C to 1500 °C. Based on the effect of both temperature and melt composition, it is thus expected that $D_{Mn}^{Ol/melt}$ in our study should be lower than the values reported by Dunn (1987). For $D_{Mn}^{Cpx/melt}$ there is a slight discrepancy between Dunn (1987) and our data. Dunn (1987) performed his experiments at P–T conditions similar to our study, and higher SiO_2 content in the melt varying between ~45 and ~50 wt.%. From our experiments we observe no significant variation of $D_{Mn}^{Cpx/melt}$ with the SiO_2 content of the melt. Dunn (1987) reports average $D_{Mn}^{Cpx/melt}$ ranging from 0.81 to 0.91 whereas our experiments yield values of 1.11 ± 0.05. The origin of the discrepancy is unclear. Walter (1998) reported $D_{Mn}^{Ol/melt}$ of ~0.72 at 3 GPa and 1530 °C. The pressure effect on$D_{Mn}^{Ol/melt}$ seems rather small since at 2 GPa and 1500 °C we measure $D_{Mn}^{Ol/melt}$ of 0.75 consistent with 3 GPa data of Walter (1998).

Co^{2+}: Similar to Zn, partition coefficients for Co have not been extensively studied. Ehlers et al. (1992), based on 1 atmosphere experiments at 1350 °C, report Co partitioning coefficients between olivine and melt (2.26–3.32) similar to our study (2.59 ± 0.57). Melt and olivine composition do not affect significantly $D_{Co}^{Ol/melt}$ in the range of P–T–X used in Ehlers et al. (1992) and in our study.

Ni^{2+}: A large number of studies report Ni partition coefficients in Earth's mantle minerals, which allow us to assess the validity of our experiments. Both temperature and melt composition have effects on Ni partitioning (e.g. Beattie, et al., 1991; Ehlers, et al., 1992; Hart and Davis, 1978; Leeman and Lindstrom, 1978; Li, et al., 2003; Li and Ripley, 2010; Wang and Gaetani, 2008). Our experiments produce mineral-melt Ni partition coefficients that are in the range of the published values for similar temperature-composition conditions.

4.2. Application to oceanic basalts—peridotite source

It has been previously suggested that Zn/Fe and Mn/Fe ratios minimally fractionate during partial melting of peridotite ($K_{DZn/Fe}^{peridotite/melt}$ ~0.8 and $K_{DMn/Fe}^{peridotite/melt}$ ~1) and olivine fractionation (Humayun, et al., 2004; Le Roux, et al., 2010; Qin and Humayun, 2008). Zn/Fe is particularly sensitive to the presence of Cpx-Gt rich lithologies (Le Roux, et al., 2010) because it fractionates significantly during partial melting of Cpx-Gt dominated lithology but stays relatively constant during partial melting of an Ol-Opx dominated lithology (peridotite). This predicts high Zn/Fe ratios in basalts produced from a Cpx-Gt rich source ($Zn/Fe \times 10^4 > 13$) whereas $Zn/Fe \times 10^4$ of MORB, produced mostly by partial melting of peridotite, usually plot between 8 and 10 (Le Roux et al. 2010). Co bulk partition coefficient between peridotite and basaltic melt is between that of Fe and Ni, which makes Co/Fe and Ni/Co ratios potential tracers of mantle source (K_Ds ~2). Similarly Mn and Zn have similar compatibilities (Le Roux et al. 2010; this study). In Fig. 7 we plotted Zn/Fe vs Mn/Fe, Co/Fe vs Mn/Fe and Ni/Co vs Mn/Zn of world-wide OIB and MORB. We only

Table 3
Partition coefficients (*Ds*) of Mn, Fe, Co, Ni and Zn between olivine, orthopyroxene, clinopyroxene and melt obtained in this study.

	P (Gpa)	T (°C)	K_D Fe/Mg	DMn	Stdev	DFe	Stdev	DCo	Stdev	DNi	Stdev	DZn	Stdev
Olivine													
G109***	1.5	1300	0.33	1.15	0.03	1.57	0.02	3.06	0.17	10.28	0.24	1.16	0.05
G107***	1.5	1325	0.33	1.03	0.04	1.41	0.03	3.08	0.03	9.13	0.24	1.02	0.06
G81*	2	1450	0.35	0.78	0.05	1.10	0.09	2.24	0,09	6.64	0.13	1.09	0.18
G84*	2	1500	0.34	0.75	0.08	1.03	0.04	1.96	0.08	5.65	0.15	0.89	0.22
Average			0.34	0.93	0.20	1.27	0.26	2.58	0.57	7.92	2.15	1.04	0.12
Average highT				0.77	0.02	1.06	0.05	2.10	0.20	6.14	0.70	0.99	0.14
Average lowT				1.09	0.09	1.49	0.11	3.07	0.01	9.70	0.82	1.09	0.10
Orthopyroxene													
G109***	1.5	1300	0.29	1.05	0.03	0.91	0.03	1.46	0.04	4.33	0.25	0.72	0.11
G110***	1.5	1310	0.29	0.98	0.02	0.86	0.03	1.42	0.04	4.44	0.25	0.70	0.04
G107***	1.5	1325	0.29	0.90	0.09	0.79	0.05	1.23	0.07	–	0.69	0.57	0.08
G90*	1.5	1375	0.30	0.85	0.04	0.74	0.04	1.30	0.08	3.60	0.14	0.77	0.13
G92*	1.5	1425	0.31	0.78	0.04	0.68	0.08	1.00	0.14	3.73	0.15	0.60	0.23
G83*	2	1400	0.36	0.78	0.05	0.75	0.04	1.04	0.11	2.77	0.39	0.75	0.30
G81*	2	1450	0.32	0.70	0.08	0.65	0.10	0.99	0.18	4.49	027	0.67	0.26
G84*	2	1500	0.31	0.66	0.15	0.63	0.03	0.89	0.19	3.88	0.29	0.63	0.27
Average			0.31	0.84	0.13	0.75	0.10	1.17	0.21	3.89	0.61	0.68	0.07
Average highT				0.75	0.08	0.69	0.05	1.04	0.15	3.69	0.62	0.68	0.07
Average lowT				0.97	0.08	0.85	0.06	1.37	0.12	4.38	0.08	0.66	0.08
Clinopyroxene													
G94**	1.5	1290	0.30	1.16	0.04	0.76	0.04	1.18	0.03	3.78	0.38	0.50	0.06
G110***	1.5	1310	0.32	1.15	0.06	0.71	0.08	1.04	0.07	3.37	0.17	0.49	0.10
G93**	1.5	1320	0.31	1.06	0.03	0.68	0.07	1.06	0.03	3.37	0.17	0.47	0.08
G107***	1.5	1325	0.34	1.08	0.08	0.68	0.06	0.96	0.06	2.44	0.50	0.44	0.08
Average			0.32	1.11	0.05	0.71	0.04	1.06	0.09	3.24	0.57	0.48	0.03

* Indicates experiments using starting composition Mix1, ** indicates experiments using starting composition Mix2, *** indicates experiments using starting composition Mix3. For Ol and Opx Ds, 'average highT' indicates the average *Ds* based on experiments at T≥1375 °C and 'average lowT' indicates the average *Ds* based on experiments at T<1375 °C.

selected primitive basalts with MgO>8.5 wt.% and we did not differentiate alkalic from tholeiitic OIB as no significant difference was observed between these two types of basalt in terms of their Zn–Mn–Fe–Co–Ni systematics.

In Fig. 7, we also plotted the transition metal ratios for DMM after Salters and Stracke (2004) and for the end member basalts HIMU, EM1 and EM2 (Table 2). The latter three end-members were estimated following the approach of Jackson and Dasgupta (2008), which relies on averaging the major and trace element chemistry of ocean island basalts that display the most extreme isotopic compositions. To account for crystal fractionation in OIB, Co and Ni contents were extrapolated to 14 wt.% MgO along the slope of a linear regression to Co- and Ni–MgO data arrays defined by individual OIB datasets. This was not necessary for Zn, Mn, and Fe because their ratios do not change significantly with fractionation in primitive basalts. For MORB, data only with MgO>8.5 wt.% are plotted. We illustrate in Fig. 7 that the majority of primitive OIB display Mn/Fe and Mn/Zn ratios lower than primitive MORB, whereas Zn/Fe ratios of OIB extend to higher values compared to MORB (Le Roux, et al., 2010). Co/Fe ratios of MORB plot in the range of OIB values.

To place these observed compositional differences in a more quantitative context, we compare these observations to models of peridotite partial melting using the bulk partition coefficients for Zn, Mn, Fe, Co and Ni. The goal is to test whether the global range of MORB, OIB and mantle end-member lavas can be derived from partial melting of peridotite (Fig. 7). The peridotite partial melting curves in Fig. 7 are calculated using a PM-like peridotite starting composition (Zn = 55 ppm; Mn = 1045 ppm; Fe = 62,600 ppm; Co = 105 ppm; and Ni = 1960 ppm; McDonough and Sun, 1995). Partial melting at 1.5 and 4 GPa was modeled by batch melting using the following equation:

$$C_l = \frac{C_o}{D_o * (1-F) + F}$$

where for a given element, C_l is its concentration in the liquid at a given melting degree F, C_o is its concentration in the initial source, and D_o is the bulk partition coefficient, $D^{element}_{peridotite/melt}$. Although melting is, in reality, controlled by fractional processes, the use of batch melting equation is sufficient as it is well-known that the composition of aggregate fractional melts is indistinguishable from batch melts (this is not the case for residues). Bulk partition coefficients for peridotite melting were calculated using mineral/melt partition coefficients from this study, spinel/melt partition coefficients from Horn et al. (1994) for Zn, Righter et al. (2006) for Ni and Co and Falloon et al. (2008) for Mn and Fe, and garnet/melt partition coefficients for all FRTEs of interest from Pertermann et al. (2004). In order to calculate bulk D at 1.5 GPa, we used modal proportions from a fertile spinel peridotite (near-solidus modes: Ol = 52%; Opx = 28%; Cpx = 19%; Sp = 1%; Falloon, et al., 2008) and 'low' temperature (<1375 °C) mineral/melt partition coefficients from this study (Table 3). For higher pressures, we used sub-solidus garnet peridotite modes from Walter (1998) (near-solidus modes: Ol = 53.6%; Opx = 5.6%; Cpx = 27.9%; and Gt = 12.9% at 4 GPa) and 'high' temperature (≥1375 °C) mineral/melt partition coefficients from this study (Table 3). We assume here that the source of MORB has a lower mantle potential temperature than the OIB sources (e.g. Herzberg, et al., 2007). In order to take into account the change in phase proportion during melting, bulk partition coefficients were calculated at specific melting degrees, using modal compositions of residues observed in Falloon et al. (2008) and Walter (1998). For peridotite melting at 1.5 GPa, we calculated the bulk Ds at 5, 10, 15 and 20% melting using the residual modes from Falloon et al. (2008). For peridotite melting at 4 GPa, we used the proportion of residues from Walter (1998) observed at 1, 10 and 13% melting. In our calculations we further assumed that the temperature change during decompression melting is small to affect mineral/melt partition coefficients of bivalent FRTEs. The parameters we used to calculate the melting trends are available in Table 1 of the Supplementary material (bulk *Ds* according to P, T, melting degrees and modal mineral proportion of residues).

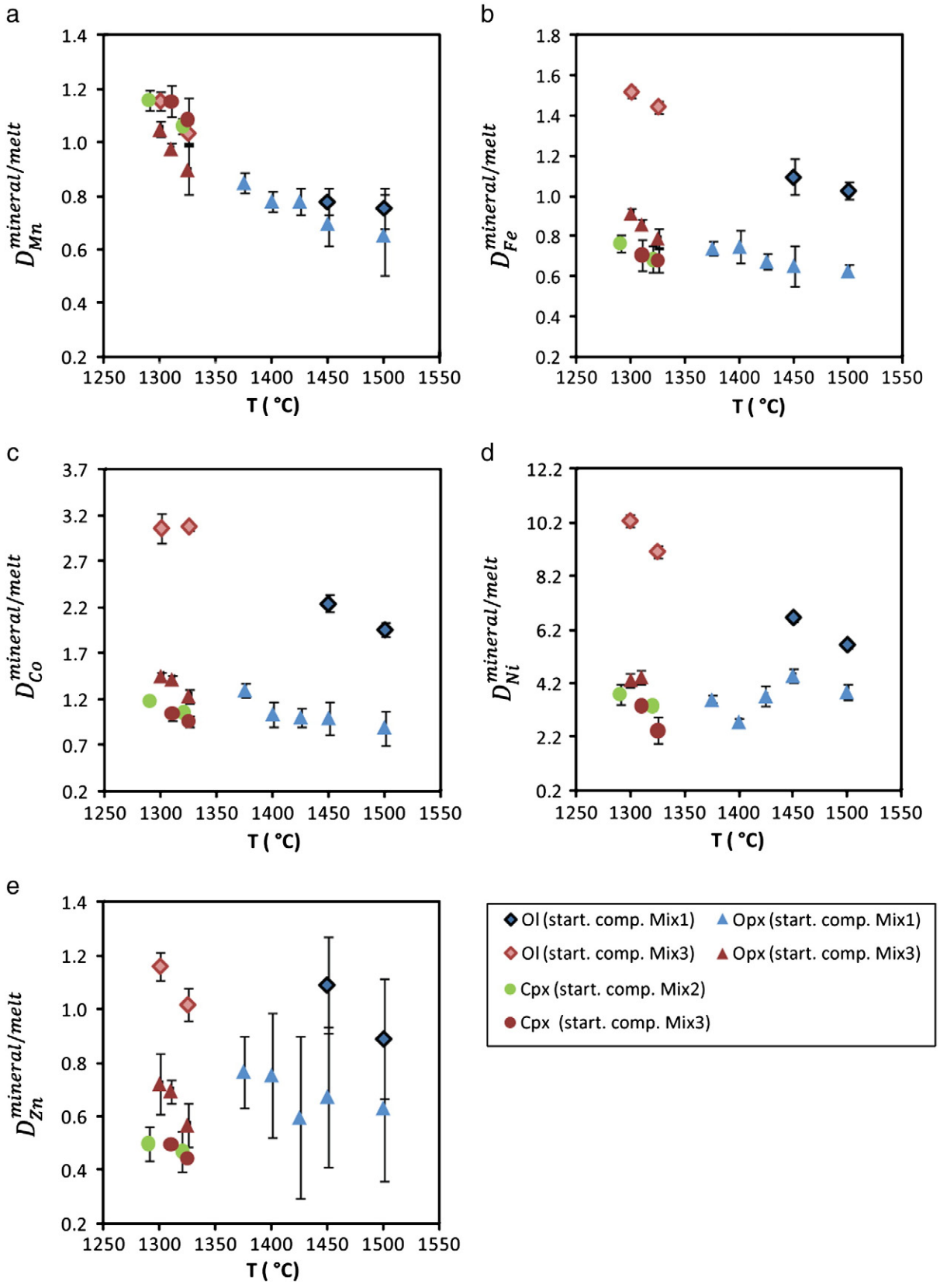

Fig. 3. Temperature dependence of mineral-melt partition coefficients (D) for Mn (a), Fe (b), Co (c), Ni (d), and Zn (e) for olivine, orthopyroxene, and clinopyroxene. The blue symbols are for experiments produced with starting composition (start. comp.) Mix1, the green symbols are for experiments with starting composition Mix2 and the red symbols are for experiments with starting composition Mix3.

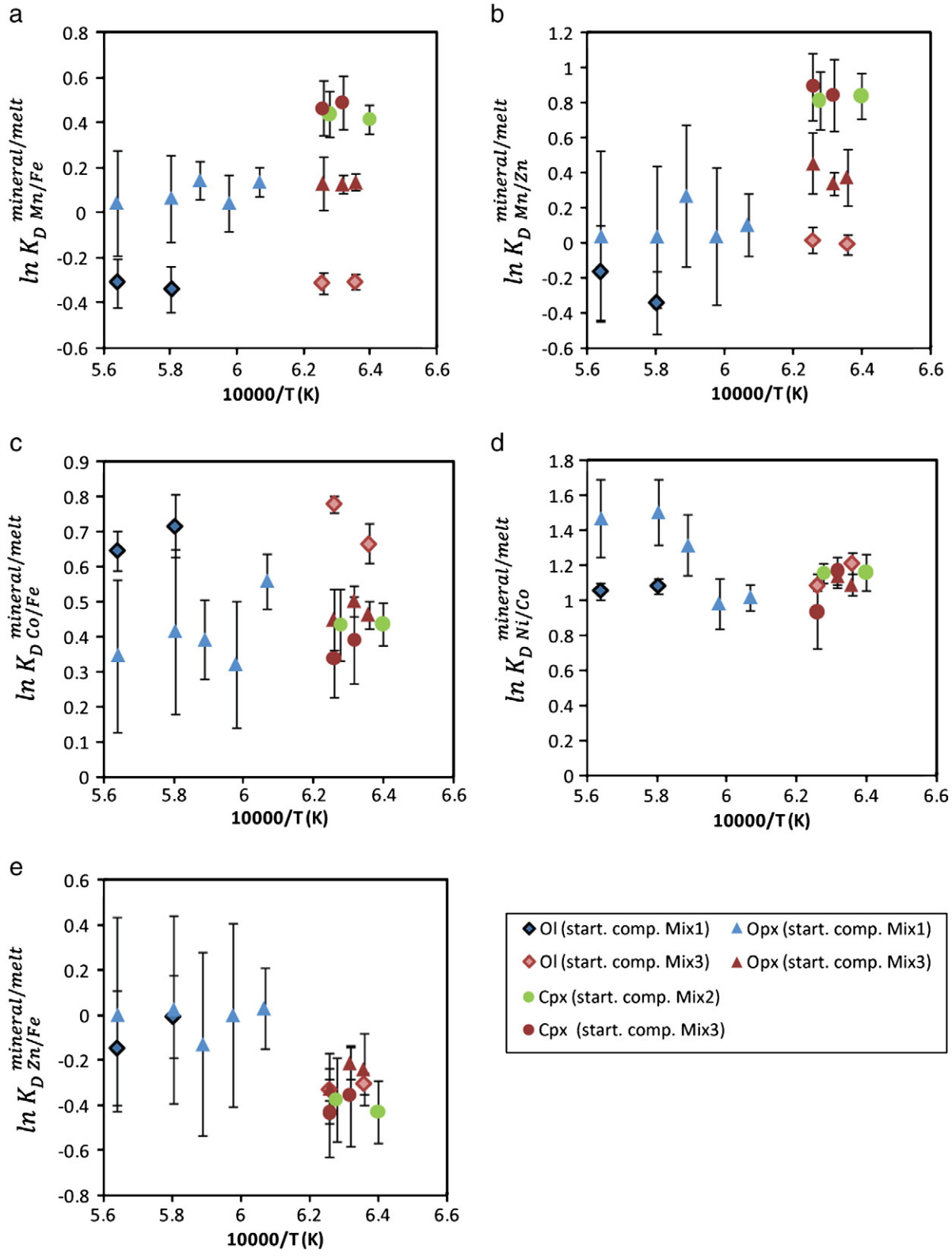

Fig. 4. Dependence of Mn/Fe (a), Mn/Zn (b), Co/Fe (c), Ni/Co (d) and Zn/Fe (e) exchange partition coefficients (K_D) between olivine, orthopyroxene, clinopyroxene and melt on reciprocal temperature. The blue symbols are mineral phases produced with starting composition (start. comp.) Mix1, the green symbols with starting composition Mix2 and the red symbols with starting composition Mix3.

On Fig. 7 we have plotted vertical and horizontal lines that mark the estimated maximum (for Zn/Fe) and estimated minimum (for Mn/Fe, Co/Fe, Ni/Co and Mn/Zn) ratios in basalts that can be derived from partial melting of a PM-like peridotite. Those lines are constrained by the range of ratios that can be derived from batch melting of peridotite, extending down to ~120–130 km depth, i.e., 4 GPa. We note that Zn/Fe ratio in peridotite-derived melt can be higher if partial melt is generated at pressures approaching 6–7 GPa owing to increased mode of garnet

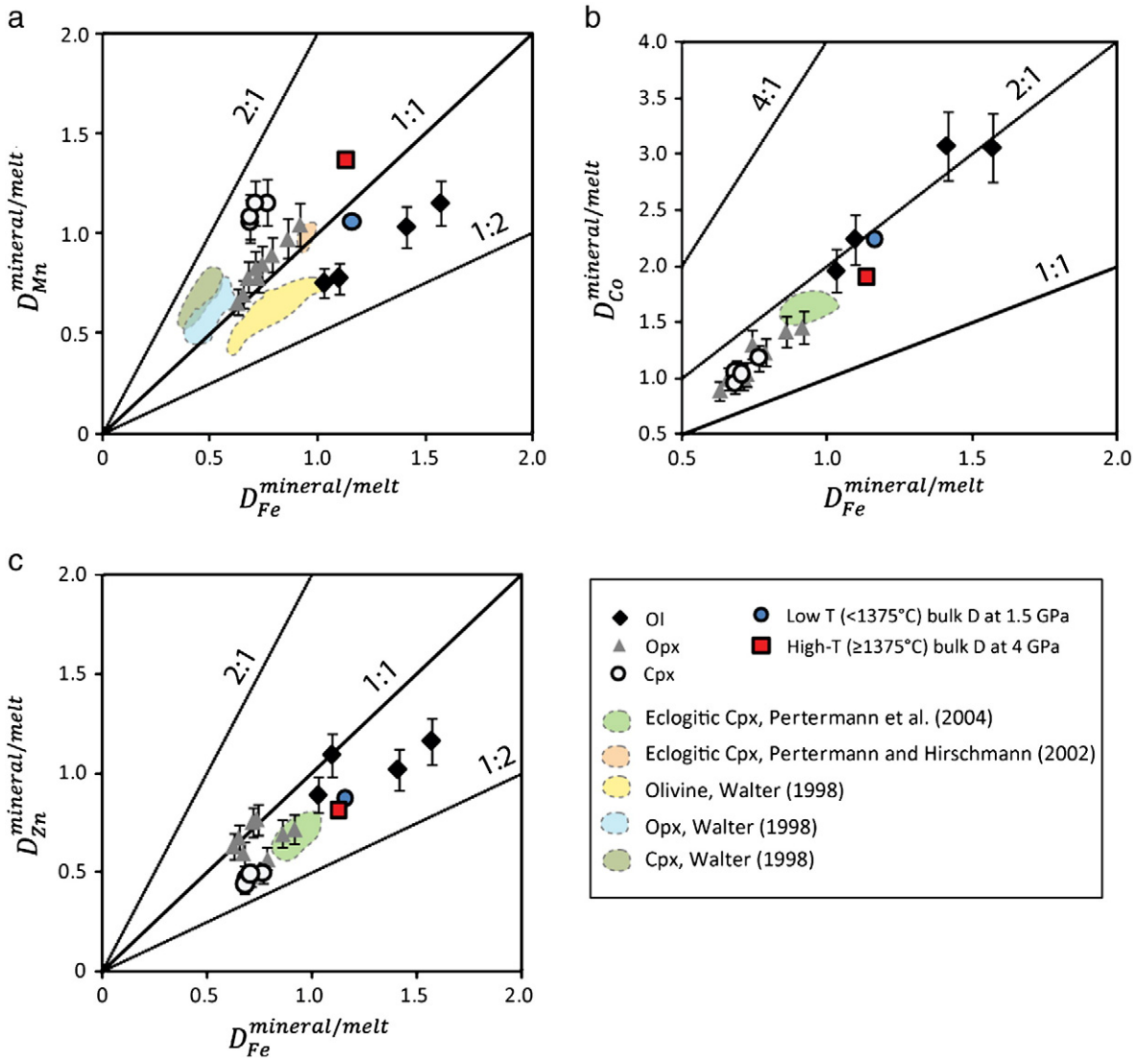

Fig. 5. Variations of D_{Mn} (a), D_{Co} (b) and D_{Zn} (c) versus D_{Fe} between olivine, orthopyroxene, clinopyroxene and melt. Literature data (Pertermann, et al., 2004; Pertermann and Hirschmann, 2002; Walter, 1998) is added for comparison. Low temperature (T <1375 °C) bulk *D*s and high temperature bulk *D*s (T≥1375 °C) between peridotite and melt have been calculated at 1.5 and 4 GPa (see text and Table 1, Supplementary material for details). Lines starting at the origin illustrate the extent of deviation of Mn–Fe, Co–Fe and Zn–Fe mineral-melt and rock-melt K_Ds from 1.

and decreased mode of Opx in near solidus peridotite, or if the peridotite has been metasomatized and enriched in Zn (Le Roux, et al., 2010). The model shown here only intends to give an estimate of FRTEs ratios in partial melts derived from a PM-like peridotite and can be recalculated for the range of Zn/Fe values observed in peridotites (~6–11). Regarding Zn/Fe, Mn/Fe, Mn/Zn and Ni/Co ratios, melts derived from a peridotite source at 1.5 GPa partly overlap with the compositional range of MORB. Some OIB such as those from Iceland, Comoros and Galapagos show FRTEs systematics consistent with melting of a primarily peridotitic source (see Supplementary material for individual islands), which may not be surprising given that Iceland and Galapagos are on or near ridge segments and are likely influenced by shallow melting of peridotite. Other OIB do not fall on the partial melting trends defined by melting of a PM-like peridotite and have Zn/Fe ratios too high or Mn/Fe, Co/Fe, Ni/Co and Mn/Zn ratios too low to be explained by partial melting of peridotite alone.

4.3. Application to oceanic basalts—heterogeneities in the peridotite source

The presence of pyroxenite or eclogite in the source of OIB has been suggested by a large number of authors based on isotopes, trace, and major elements constraints (e.g., Christensen and Hofmann, 1994; Herzberg, 2006; Hofmann and White, 1982; Jackson and Dasgupta, 2008). In the following discussion, we argue that the presence of such lithologies can provide a reasonable solution to the FRTEs chemistry of OIB and MORB. We investigate the effects of eclogite melting on OIB compositions using a typical MORB-like eclogite source (Zn = 75 ppm; Mn = 1239 ppm; Fe = 80,063 ppm; and Co = 80 ppm; Arevalo and McDonough, 2010). Fig. 7 plots the predicted partial melting trend defined by melting of MORB-like eclogite with ~82% Cpx and ~18% Gt (Pertermann and Hirschmann, 2003) in Zn/Fe versus Mn/Fe, Co/Fe versus Mn/Fe, and Ni/Co versus Mn/Zn spaces. Our melting calculations for eclogites follow the same approach used above for peridotite melting. We used $D^{Gt/melt}$ and $D^{Cpx/melt}$ from Pertermann et al. (2004) and the modal compositions of residues from Pertermann and Hirschmann (2003) in a MORB-like eclogite melting at 3, 36, 60 and 80% at 3 GPa. It can be seen that a large proportion of the OIB data (and MORB data in terms of Ni/Co and Co/Fe) can be explained by mixing of partial melts from eclogitic and peridotitic sources or by addition of eclogitic melts to peridotitic source and then re-melting of the metasomatized source. For example, melting of eclogite predicts negative

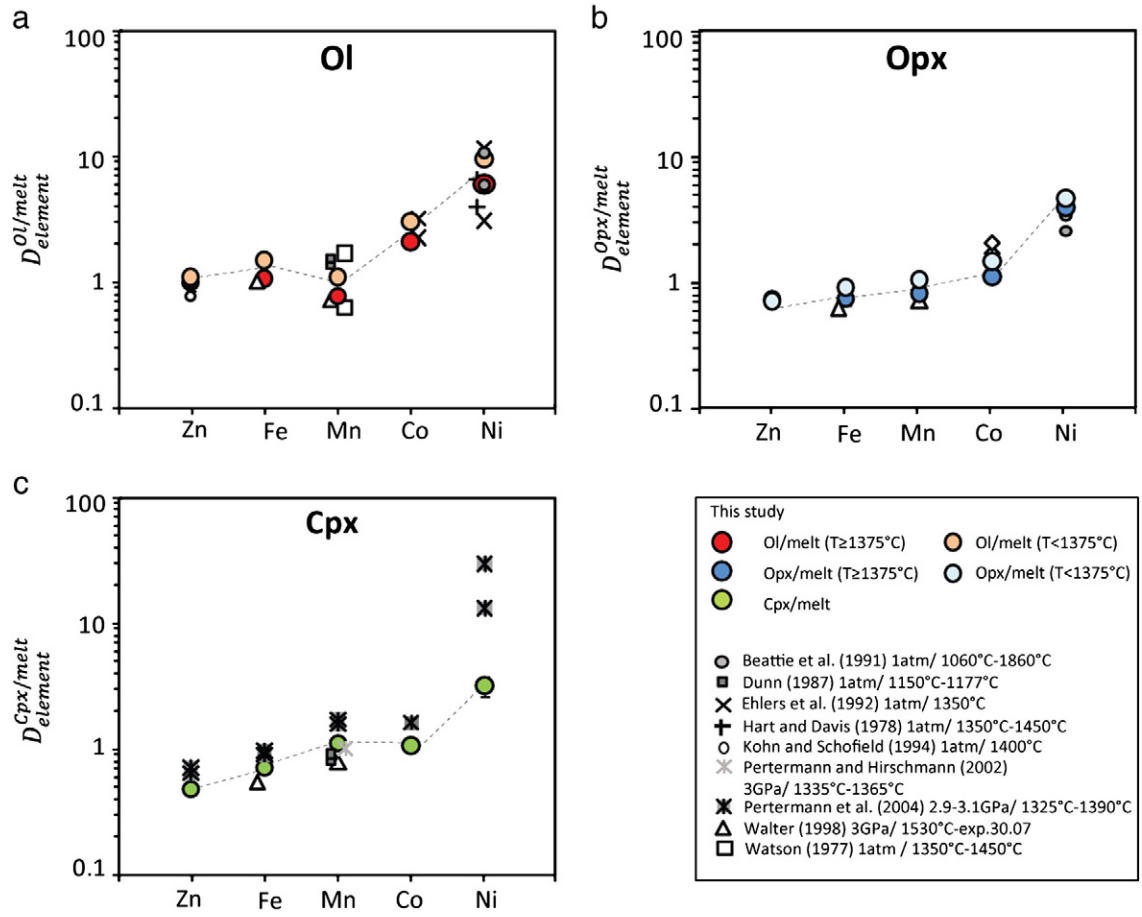

Fig. 6. Averages of high-T (≥1375 °C) and low-T (<1375 °C) olivine-melt (a), Opx-melt (b) and Cpx-melt (c) partition coefficients from this study compared to literature experimental data (plotted are the higher and lower value of the range of values) (Beattie, et al., 1991; Dunn, 1987; Ehlers, et al., 1992; Hart and Davis, 1978; Kohn and Schofield, 1994; Pertermann, et al., 2004; Pertermann and Hirschmann, 2002; Walter, 1998; Watson, 1977). The plotted $D_{Ni}^{Ol/melt}$ data from Beattie et al. (1991) are estimated using $D_{Mg}^{Ol/melt}$ for both high temperature (≥1375 °C) and low temperature (<1375 °C) experiments. Symbols are bigger than the error bars where no error bars (one standard deviation of the average, see Table 3) are visible.

correlation between Mn/Fe and Zn/Fe, which is consistent with the OIB data.

To quantify the contribution of eclogite-derived melt in the erupted basalts we present a model melt–melt mixing calculation with assumptions about effective melting degrees in peridotite and eclogite. In this example we adopt a MORB composition for the eclogite end-member in the mantle and assume that the eclogite is composed of 82% Cpx-18% Gt. We note that other types of "eclogitic" lithologies are certainly possible, but the purpose of this discussion is to evaluate geochemical trends imparted by melting of Gt + Cpx lithologies rather than model every type of lithological heterogeneity in the mantle. We assume that the mantle represents a mechanical mixture of eclogite and peridotite below the solidi of both the lithologies and upon melting the partial melts from both the lithologies mix. However, because the solidi of these two components are not the same, they do not contribute equally to the aggregate melt. We assume that the peridotite starts melting when eclogite approaches 60% melting (approximation from the experiments at 3 GPa by Pertermann and Hirschmann, 2003) but we do not include any melt-rock reaction step (e.g., Sobolev et al., 2005, 2007) in our model. We do not suggest that such reactions do not happen, but a detailed evaluation of the role of melt-rock reaction on the FRTEs compositions of basalts is beyond the scope of this study. Thus our model is a simplification of natural systems and the model will vary according to the solidus of the peridotite and eclogite chosen and extent of melt-rock reaction. The purpose of our model is only to show the relative contributions of eclogite versus peridotite partial melts in the erupted basalts of various ocean islands. The mixing lines of Fig. 7 allow estimating the contribution of eclogite versus peridotite-derived melt of any lava and the degree of melting associated with both lithologies. By comparing the data to predicted mixing lines, we can then quantify the proportion of eclogite (used in this model) present, for instance, in the source of the mantle end-members with the following equation.

$$A_{ecl} = X_{ecl} \times 100 / \left(X_{ecl} + X_{per} \right)$$

where A_{ecl} is the percentage of eclogite in the source, $X_{ecl} = (X_{melt\ ecl}/F_{ecl})$, where $X_{melt\ ecl}$ is the fraction of eclogite-derived melts in the aggregate melt, and F_{ecl} the degree of melting of eclogite; $X_{per} = (X_{melt\ per}/F_{per})$ where $X_{melt\ per}$ is the fraction of peridotite-derived melts in the aggregate melt and F_{per} the degree of melting of peridotite.

One of the advantages of using independent sets of ratios (e.g. Zn/Fe–Mn/Fe and Ni/Co–Mn/Zn) is that we can assess whether our estimates of the proportion of eclogite in the source of mantle-derived basalts are internally consistent. Estimations for EM1 and HIMU are fairly consistent throughout the three panels on Fig. 7. For instance, EM1 FRTEs systematics could have been generated by mixing ~30% eclogite partial melts ($F_{ecl} = 60\%$) and ~70% peridotite partial melt at 4 GPa ($F_{per} = 1\%$). This corresponds to a proportion of eclogite in the mantle of A_{ecl} ~1%. Similarly, HIMU could be generated by mixing of ~30 to 60% eclogite partial melt ($F_{ecl} = 80\%$) and ~40 to 70% peridotite partial melt at 4 GPa ($F_{per} = 13\%$), which would yield A_{ecl} ~10–20%. Those estimate

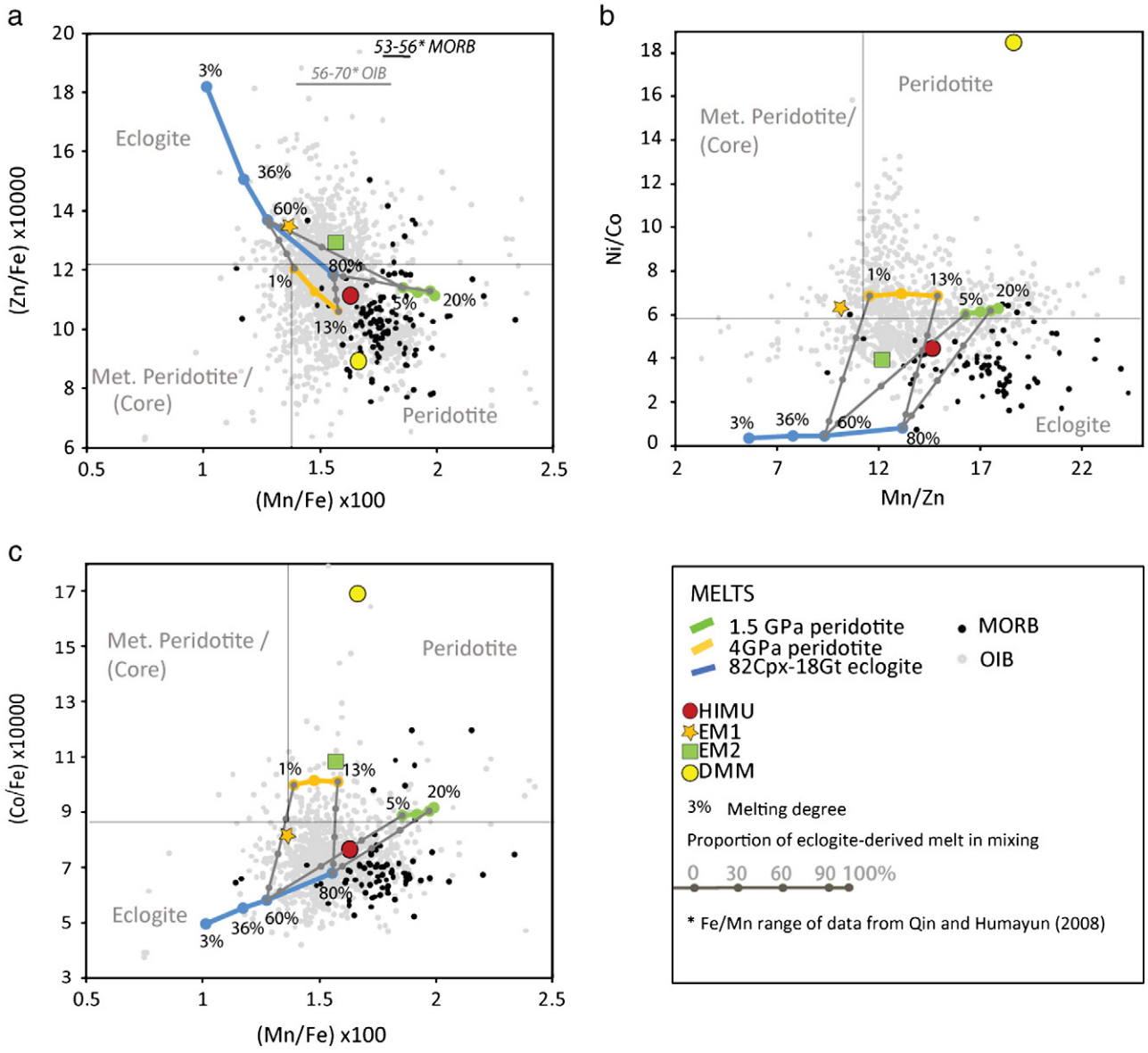

Fig. 7. $Zn/Fe \times 10^4$ vs $Mn/Fe \times 100$ (a), Ni/Co vs Mn/Zn (b) and Co/Fe vs $Mn/Fe \times 100$ (c) in MORB, OIB, mantle end-member DMM, and mantle end-members basalts HIMU, EM1, and EM2. OIB have been corrected to MgO = 14 wt.% and MORB have MgO > 8.5 wt.%. 1.5 GPa and 4 GPa lines are partial melting trend of a PM-like peridotite. Blue line is the partial melting trend of an eclogite composed of 82% Cpx-18% Gt. The gray lines are mixing lines between eclogite-derived and peridotite-derived melts. The quadrant domains indicate what could be the main additional lithology associated with peridotite in the source of mantle-derived basalts. The vertical and horizontal lines mark the maximum (for Zn/Fe) and minimum (for Mn/Fe, Co/Fe, Ni/Co and Mn/Zn) ratios in basalts that can be derived from partial melting of a PM-like peridotite assuming that oceanic basalts beneath ridges and ocean islands are derived from pressures ≤4 GPa. The black and gray lines with numbers in italics at the top of Fig. 7a indicate the range of high-precision Fe/Mn values measured in MORB and OIB (Iceland, St Helena, Tahiti and Reunion) by Qin and Humayun (2008).

(even though model dependent) show that in most cases the combination of several FRTEs ratios may bring fairly consistent information on the amount of Cpx-Gt rich lithologies in the source of mantle end-members. We note that estimations for EM2 are more problematic, Zn/Fe vs Mn/Fe and Ni/Co vs Mn/Zn plots would indicate that EM2 could for instance be generated by mixing of ~50% eclogite partial melt ($F_{ecl} = 60\%$) and ~50% peridotite partial melt at 1.5 GPa ($F_{per} = 5\%$), which would yield A_{ecl} ~8%, however Co/Fe of EM2 is too high to be explained as such. We believe that discrepancies observed on the amount of eclogite in the mantle end-members could come from the fact that the FRTEs ratios of mantle end-members are not well constrained or that the correction to primitive magmas can be improved. It is beyond the scope of this study to constrain the FRTEs contents of individual OIB, but if this can be achieved, the accuracy of the model could better be assessed.

Zn/Fe, Mn/Fe, Co/Fe, Ni/Co and Mn/Zn transition metal ratios show that varying quantities of eclogites are needed in the source of most OIB lavas such as the Society Islands, Marquesas, Hawaii etc. (Supplementary material). Even MORB and OIB associated with ridge environment (e.g. Iceland) show a hint of mixing with an eclogitic component (e.g. Sobolev et al. 2007) but are associated with peridotite melted at shallow pressures (1.5 GPa).

Finally, it is worth considering the effect of outer core contamination on deep-seated OIB mantle source regions as suggested by Humayun et al. (2004). In Fig. 7 we have distinguished several domains where we indicate what the main additional lithology potentially associated with peridotite in the source of basalts. The 'peridotite' and 'eclogite' fields have been drawn using our partial melting models, and the 'core' field corresponds to that expected for a hypothetical contribution from the liquid outer core as suggested by Humayun et al. (2004). We can

approximate how a contribution from liquid outer core would modify the Zn/Fe, Mn/Fe, Co/Fe, Ni/Co and Mn/Zn ratios of basalts using the estimated bulk core composition from McDonough, (2003). For instance, assuming mechanical mixing at the core-mantle boundary, we would expect that a core contribution would decrease both the Zn/Fe and Mn/Fe ratios of mantle-derived basalts as the core contains 85.5 wt.% of Fe ($Zn/Fe \times 10^4 = 0.35$ if we use a maximum of 30 ppm Zn in the core from Corgne, et al., 2008; $Mn/Fe \times 100 = 0.035$). We would also expect lavas to display high Co/Fe ratios ($Co/Fe_{core} \times 10^4 = 29$) associated with low Mn/Fe. Ni/Co ratio would also be expected to be high as its value in the Earth's core is 20.8 while Mn/Zn ($= 10$ if $Zn = 30$ ppm) would be minimally affected. It can be seen that core-contamination fails to explain all the transition metal systematics simultaneously.

5. Concluding remarks

In this study we present internally consistent partitioning data of first-row divalent transition metals Mn^{2+}, Fe^{2+}, Co^{2+} and Ni^{2+} between olivine, orthopyroxene, clinopyroxene and basaltic melt at shallow upper mantle conditions ($P = 1.5$–2 GPa and $T = 1300$–1500 °C). It is also the first experimental study of Zn^{2+} partitioning and Zn/Fe exchange between peridotite minerals (olivine, orthopyroxene, and clinopyroxene) and basaltic melts at conditions relevant for oceanic basalt source regions. We have combined multiple divalent FRTEs tracers in order to better constrain the mineralogical composition of the source regions of basalts. We show that, because of their moderately incompatible to compatible behavior, these elements are promising tracers of lithological heterogeneities in the source regions of basalts. We have combined our partitioning data (*Ds*) for Ol-melt, Opx-melt, and Cpx-melt, with previous studies on spinel-melt and garnet-melt partitioning to constrain bulk partition coefficients during mantle melting. In particular, we observe that melts of eclogites (Cpx + Gt rich lithologies) would be expected to have low Mn/Fe, Co/Fe, Ni/Co, Mn/Zn and high Zn/Fe compared to peridotite (Ol + Opx rich lithologies) partial melts.

We have compared data of natural oceanic basalts (MORB and OIB) with estimates of peridotite and eclogite partial melt compositions in Zn/Fe versus Mn/Fe, Co/Fe versus Mn/Fe and Ni/Co versus Mn/Zn spaces to quantify the distribution of Cpx-Gt rich heterogeneities in the mantle source. We have used a simple melting and melt–melt mixing model to quantify the amount of MORB-like eclogite in the source of individual ocean islands, and despite the simplifications and limitations of the model, the combined FRTEs ratios appear to be able to yield consistent results on the source composition.

Acknowledgments

We are grateful to Ray Guillemette for his assistance with electron microprobe analyses at Texas A&M University. We thank two anonymous reviewers for their thoughtful and constructive reviews that helped us improve the manuscript and Lars Stixrude for editorial handling. The work received support from NSF grant EAR-0911442 to RD, from Packard Fellowships to R.D. and C.-T. L. and from the Postdoctoral Scholar Program at the Woods Hole Oceanographic Institution, with funding provided by the Deep Ocean Exploration Institute, to V.L.R.

Appendix A. Supplementary data

Supplementary data to this article can be found online at doi:10.1016/j.epsl.2011.05.014.

References

Arevalo, R., McDonough, W.F., 2010. Chemical variations and regional diversity observed in MORB. Chem. Geol. 271, 70–85.
Beattie, P., Ford, C., Russell, D., 1991. Partition coefficients for olivine-melt and orthopyroxene-melt systems. Contrib. Mineral. Petrol. 109, 212–224.
Christensen, U.R., Hofmann, A.W., 1994. Segregation of subducted oceanic crust in the convecting mantle. J. Geophys. Res. 99, 19867–19884.
Corgne, A., Keshav, S., Wood, B.J., McDonough, W.F., Fei, Y.W., 2008. Metal-silicate partitioning and constraints on core composition and oxygen fugacity during Earth accretion. Geochim. Cosmochim. Acta 72, 574–589.
Dasgupta, R., Hirschmann, M.M., Smith, N.D., 2007. Partial melting experiments of peridotite CO2 at 3 GPa and genesis of alkalic ocean island basalts. J. Petrol. 48, 2093–2124.
Dasgupta, R., Hirschmann, M.M., Stalker, K., 2006. Immiscible transition from carbonate-rich to silicate-rich melts in the 3 GPa melting interval of eclogite plus CO2 and genesis of silica-undersaturated ocean island lavas. J. Petrol. 47, 647–671.
Dasgupta, R., Jackson, M.G., Lee, C.-T.A., 2010. Major element chemistry of ocean island basalts—conditions of mantle melting and heterogeneity of mantle source. Earth Planet. Sci. Lett. 289, 377–392.
Dunn, T., 1987. Partitioning of Hf, Lu, Ti and Mn between olivine, clinopyroxene and basaltic liquid. Contrib. Mineral. Petrol. 96, 476–484.
Ehlers, K., Grove, T.L., Sisson, T.W., Recca, S.I., Zervas, D.A., 1992. The effect of oxygen fugacity on the partitioning of nickel and cobalt between olivine, silicate melt, and metal. Geochim Cosmochim. Acta 56, 3733–3743.
Falloon, T.J., Green, D.H., Danyushevsky, L.V., McNeill, A.W., 2008. The composition of near-solidus partial melts of fertile peridotite at 1 and 1.5 GPa: implications for the petrogenesis of MORB. J. Petrol. 49, 591–613.
Gao, S., Liu, X.M., Yuan, H.L., Hattendorf, B., Gunther, D., Chen, L., Hu, S.H., 2002. Determination of forty two major and trace elements in USGS and NIST SRM glasses by laser ablation-inductively coupled plasma-mass spectrometry. Geostand. Newsl. 26, 181–196.
Gerbode, C., Dasgupta, R., 2010. Carbonate-fluxed melting of MORB-like pyroxenite at 2.9 GPa and genesis of HIMU ocean island basalts. J. Petrol. 51, 2067–2088.
Hart, S.R., Davis, K.E., 1978. Nickel partitioning between olivine and silicate melt. Earth Planet. Sci. Lett. 40, 203–219.
Herzberg, C., 2006. Petrology and thermal structure of the Hawaiian plume from Mauna Kea volcano. Nature 444, 605–609.
Herzberg, C., Asimow, P.D., Arndt, N., Niu, Y.L., Lesher, C.M., Fitton, J.G., Cheadle, M.J., Saunders, A.D., 2007. Temperatures in ambient mantle and plumes: constraints from basalts, picrites, and komatiites. Geochem. Geophys. Geosyst. 8, 34.
Hirschmann, M.M., Kogiso, T., Baker, M.B., Stolper, E.M., 2003. Alkalic magmas generated by partial melting of garnet pyroxenite. Geology 31, 481–484.
Hirschmann, M.M., Stolper, E.M., 1996. A possible role for garnet pyroxenite in the origin of the "garnet signature" in MORB. Contrib. Mineral. Petrol. 124, 185–208.
Hofmann, A.W., 1997. Mantle geochemistry: the message from oceanic volcanism. Nature 385, 219–229.
Hofmann, A.W., White, W.M., 1982. Mantle plumes from ancient oceanic-crust. Earth Planet. Sci. Lett. 57, 421–436.
Horn, I., Foley, S.F., Jackson, S.E., Jenner, G.A., 1994. Experimentally determined partitioning of high field strength- and selected transition elements between spinel and basaltic melt. Chem. Geol. 117, 193–218.
Humayun, M., Qin, L.P., Norman, M.D., 2004. Geochemical evidence for excess iron in the mantle beneath Hawaii. Science 306, 91–94.
Jackson, M.G., Dasgupta, R., 2008. Compositions of HIMU, EM1, and EM2 from global trends between radiogenic isotopes and major elements in ocean island basalts. Earth Planet. Sci. Lett. 276, 175–186.
Kinzler, R.J., 1997. Melting of mantle peridotite at pressures approaching the spinel to garnet transition: application to mid-ocean ridge basalt petrogenesis. J. Geophys. Res. 102, 853–874.
Kinzler, R.J., Grove, T.L., 1992. Primary magmas of mid-ocean ridge basalts.1. Experiments and methods. J. Geophys. Res. 97, 6885–6906.
Kogiso, T., Hirose, K., Takahashi, E., 1998. Melting experiments on homogeneous mixtures of peridotite and basalt: application to the genesis of ocean island basalts. Earth Planet. Sci. Lett. 162, 45–61.
Kogiso, T., Hirschmann, M.M., 2006. Partial melting experiments of bimineralic eclogite and the role of recycled mafic oceanic crust in the genesis of ocean island basalts. Earth Planet. Sci. Lett. 249, 188–199.
Kogiso, T., Hirschmann, M.M., Frost, D.J., 2003. High-pressure partial melting of garnet pyroxenite: possible mafic lithologies in the source of ocean island basalts. Earth Planet. Sci. Lett. 216, 603–617.
Kohn, S.C., Schofield, P.F., 1994. The importance of melt composition in controlling trace-element behavior—an experimental study of Mn and Zn partitioning between forsterite and silicate melts. Chem Geol. 117, 73–87.
Kushiro, I., 2001. Partial melting experiments on peridotite and origin of mid-ocean ridge basalt. Annu. Rev. Earth Planet. Sci. 29, 71–107.
Kushiro, I., Walter, M.J., 1998. Mg–Fe partitioning between olivine and mafic–ultramafic melts. Geophys. Res. Lett. 25, 2337–2340.
Le Roux, V., Lee, C.T.A., Turner, S.J., 2010. Zn/Fe systematics in mafic and ultramafic systems: implications for detecting major element heterogeneities in the Earth's mantle. Geochim. Cosmochim. Acta 74, 2779–2796.
Lee, C.T.A., Luffi, P., Le Roux, V., Dasgupta, R., Albarede, F., Leeman, W.P., 2010. The redox state of arc mantle using Zn/Fe systematics. Nature 468, 681–685.
Lee, C.T.A., Oka, M., Luffi, P., Agranier, A., 2008. Internal distribution of Li and B in serpentinites from the Feather River Ophiolite, California, based on laser ablation inductively coupled plasma mass spectrometry. Geochem. Geophys. Geosyst. 9, 14. doi:10.1029/2008GC002078.
Leeman, W.P., Lindstrom, D.J., 1978. Partitioning of Ni2+ between basaltic and synthetic melts and olivines—an experimental study. Geochim. Cosmochim. Acta 42, 801–816.
Li, C., Ripley, E.M., Mathez, E.A., 2003. The effect of S on the partitioning of Ni between olivine and silicate melt in MORB. Chem. Geol. 201, 295–306.

Li, C.S., Ripley, E.M., 2010. The relative effects of composition and temperature on olivine-liquid Ni partitioning: statistical deconvolution and implications for petrologic modeling. Chem. Geol. 275, 99–104.
Longerich, H.P., Gunther, D., Jackson, S.E., Longerich, H.P., Gunther, D., Jackson, S.E., 1996. Elemental Fractionation in Laser Ablation Inductively Coupled Plasma Mass Spectrometry. Springer Verlag, pp. 538–542.
McDonough, W.F., 2003. Compositional model for the Earth's core. In: Carlson, R.W. (Ed.), The Mantle and Core—Treatise on Geochemistry Vol. 2. Elsevier, pp. 547–568.
McDonough, W.F., Sun, S.-S., 1995. The composition of the Earth. Chem. Geol. 120, 223–253.
Medard, E., McCammon, C.A., Barr, J.A., Grove, T.L., 2008. Oxygen fugacity, temperature reproducibility, and H2O contents of nominally anhydrous piston-cylinder experiments using graphite capsules. Am. Miner. 93, 1838–1844.
Niu, Y., O'Hara, M.J., 2003. Origin of ocean island basalts: a new perspective from petrology, geochemistry and mineral physics considerations. J. Geophys. Res. 108, 2209. doi:10.1029/2002JB002048.
Parman, S.W., Grove, T.L., 2004. Harzburgite melting with and without H2O: experimental data and predictive modeling. J. Geophys. Res. 109, 20.
Pertermann, M., Hirschmann, M.M., 2002. Trace-element partitioning between vacancy-rich eclogitic clinopyroxene and silicate melt. Am. Miner. 87, 1365–1376.
Pertermann, M., Hirschmann, M.M., 2003. Partial melting experiments on a MORB-like pyroxenite between 2 and 3 GPa: constraints on the presence of pyroxenite in basalt source regions from solidus location and melting rate. J. Geophys. Res. 108, 17.
Pertermann, M., Hirschmann, M.M., Hametner, K., Gunther, D., Schmidt, M.W., 2004. Experimental determination of trace element partitioning between garnet and silica-rich liquid during anhydrous partial melting of MORB-like eclogite. Geochem. Geophys. Geosyst. 5, 23.
Pilet, S., Baker, M.B., Stolper, E.M., 2008. Metasomatized lithosphere and the origin of alkaline lavas. Science 320, 916–919.
Pilet, S., Hernandez, J., Sylvester, P., Poujol, M., 2005. The metasomatic alternative for ocean island basalt chemical heterogeneity. Earth Planet. Sci. Lett. 236, 148–166.
Prytulak, J., Elliott, T., 2007. TiO2 enrichment in ocean island basalts. Earth Planet. Sci. Lett. 263, 388–403.
Qin, L.P., Humayun, M., 2008. The Fe/Mn ratio in MORB and OIB determined by ICP-MS. Geochim. Cosmochim. Acta 72, 1660–1677.
Righter, K., Leeman, W.P., Hervig, R.L., 2006. Partitioning of Ni, Co and V between spinel-structured oxides and silicate melts: importance of spinel composition. Chem. Geol. 227, 1–25.
Roeder, P.L., Emslie, R.F., 1970. Olivine-liquid equilibrium. Contrib. Mineral. Petrol. 29, 275–289.
Salters, V.J.M., Stracke, A., 2004. Composition of the depleted mantle. Geochem. Geophys. Geosyst. 5, 27.
Sobolev, A.V., Hofmann, A.W., Kuzmin, D.V., Yaxley, G.M., Arndt, N.T., Chung, S.L., Danyushevsky, L.V., Elliott, T., Frey, F.A., Garcia, M.O., Gurenko, A.A., Kamenetsky, V.S., Kerr, A.C., Krivolutskaya, N.A., Matvienkov, V.V., Nikogosian, I.K., Rocholl, A., Sigurdsson, I.A., Sushchevskaya, N.M., Teklay, M., 2007. The amount of recycled crust in sources of mantle-derived melts. Science 316, 412–417.
Sobolev, A.V., Hofmann, A.W., Sobolev, S.V., Nikogosian, I.K., 2005. An olivine-free mantle source of Hawaiian shield basalts. Nature 434, 590–597.
Spandler, C., Yaxley, G., Green, D.H., Scott, D., 2010. Experimental phase and melting relations of metapelite in the upper mantle: implications for the petrogenesis of intraplate magmas. Contrib. Mineral. Petrol. 160, 569–589.
Tsuno, K., Dasgupta, R., 2011. Melting phase relation of nominally anhydrous, carbonated pelitic–eclogite at 2.5–3.0 GPa and deep cycling of sedimentary carbon. Contrib. Mineral. Petrol. 743–763.
Walter, M.J., 1998. Melting of garnet peridotite and the origin of komatiite and depleted lithosphere. J. Petrol. 39, 29–60.
Wang, Z.R., Gaetani, G.A., 2008. Partitioning of Ni between olivine and siliceous eclogite partial melt: experimental constraints on the mantle source of Hawaiian basalts. Contrib. Mineral. Petrol. 156, 661–678.
Wasylenki, L.E., Baker, M.B., Kent, A.J.R., Stolper, E.M., 2003. Near-solidus melting of the shallow upper mantle: partial melting experiments on depleted peridotite. J. Petrol. 44, 1163–1191.
Watson, E.B., 1977. Partitioning of manganese between forsterite and silicate liquid. Geochim Cosmochim. Acta 41, 1363–1374.
Weaver, B.L., 1991. The origin of ocean island basalt end-member compositions—trace-element and isotopic constraints. Earth Planet. Sci. Lett. 104, 381–397.
Willbold, M., Stracke, A., 2006. Trace element composition of mantle end-members: implications for recycling of oceanic and upper and lower continental crust. Geochem. Geophys. Geosyst. 7, 30.
Zindler, A., Hart, S., 1986. Chemical geodynamics. Annu. Rev. Earth Planet. Sci. 14, 493–571.